Ion energy increase in laser-generated plasma expanding through axial magnetic field trap

L. TORRISI,[1,2] D. MARGARONE,[1,2] S. GAMMINO,[2] AND L. ANDÒ[2]

[1]Dipartimento di Fisica, Università di Messina, Messina, Italy
[2]INFN-Laboratori Nazionali del Sud, Catania, Italy

Abstract

Laser-generated plasma is obtained in high vacuum (10^{-7} mbar) by irradiation of metallic targets (Al, Cu, Ta) with laser beam with intensities of the order of 10^{10} W/cm^2. An Nd:Yag laser operating at 1064 nm wavelength, 9 ns pulse width, and 500 mJ maximum pulse energy is used. Time of flight measurements of ion emission along the direction normal to the target surface were performed with an ion collector. Measurements with and without a 0.1 Tesla magnetic field, directed along the normal to the target surface, have been taken for different target-detector distances and for increasing laser pulse intensity. Results have demonstrated that the magnetic field configuration creates an electron trap in front of the target surface along the axial direction. Electric fields inside the trap induce ion acceleration; the presence of electron bundles not only focuses the ion beam but also increases its energy, mean charge state and current. The explanation of this phenomenon can be found in the electric field modification inside the non-equilibrium plasma because of an electron bunching that increases the number of electron-ion interactions. The magnetic field, in fact, modifies the electric field due to the charge separation between the clouds of fast electrons, many of which remain trapped in the magnetic hole, and slow ions, ejected from the ablated target; moreover it increases the number of electron-ion interactions producing higher charge states.

Keywords: Electron trapping; Laser-generated plasma; Plasma in magnetic field

1. INTRODUCTION

In the last ten years, many experiments with laser-generated plasma have been carried out; time-of-flight (TOF) measurements of charged particles ejected from the irradiated target have been obtained by means of different pulsed lasers, and experimental setups (Alti & Khare, 2006; Beilis, 2007). Laser-generated plasma shows high temperature and density during the laser pulse irradiation and a plasma plume directed along the normal to the target surface, expanding in vacuum at supersonic velocity (Giulietti & Gizzi, 1998; Schaumann *et al.*, 2005; Jungwirth, 2005). At the laser pulse intensity on the order of 10^{10} W/cm^2 and pulse duration on the order of $1-10$ ns, generally for the ion and electron detection Faraday cups with polarized ion collectors, semiconductor detectors and electric and/or magnetic deflection analyzers are used. Ion and electron currents, ion and electron energies, ion charge states and energy distributions have been measured in different conditions and reported in

many publications (Laska *et al.*, 2006). Results demonstrate that hot electrons and fast ions with high charge state and kinetic energies can be produced by pulsed lasers irradiating solid targets. A 9 ns Nd:Yag laser operating at 800 mJ pulse energy and focused in a sub-millimeter spot on metal surfaces may produce hot electrons with average energy of the order of hundreds eV, ion energies from about 100 eV up to 5 keV, and charge states up to about 10^+ (Torrisi *et al.*, 2002). Measurements with an ion energy analyzer have demonstrated that the distributions are Boltzmann-like and that they are shifted toward high energy with the increasing laser intensity and/or ion charge state. This last result is relevant because it explains the distribution shifts with the Coulombian acceleration due to an equivalent voltage developed inside the laser-generated plasma. This voltage, V_0, is due to a temporary ($\sim$ ns) negative space charge distribution created in front of the target surface, generated by a fast electron cloud expanding from the target surface toward the normal target direction, and leaving behind a positive cloud of slower ions emitted from the target. Recent measurements demonstrated that at 10^{10} W/cm^2 this equivalent voltage is on the order of 400 V and that this voltage

grows with the laser pulse intensity (Torrisi & Gammino, 2006). Moreover, at this laser intensity, the equivalent plasma temperature and density are on the order of 200 eV and $10^{17}/cm^3$, respectively, corresponding to a Debye length of about 0.33 μm. Assuming that the equivalent voltage is applied over a distance on the order of the Debye length, the calculated electric field is about 12 MV/cm (Davis *et al.*, 1999). This high value of electric field explains the high kinetic energy acquired by the ions at high charge state ejected from the plasma.

The application of a high magnetic field to the plasma plume region, in front of the target surface, alters the linear trajectories of charged particles ejected from plasma in vacuum and modifies the resulting electric field accelerating emitted ions (Anderson *et al.*, 2005). Ducruet *et al.* (2006) demonstrated that the magnetic field confinement of the laser-generated plasma increases significantly, the deposition rate of thin films occurring on substrates placed along the normal target direction, increases the recombination effects due to the higher plasma density and decreases the mean energy of the ions.

Wolowski *et al.* (2002, 2004) demonstrated that the magnetic field causes a significant increase in the current density of the ions that expand in the magnetic field axis. Moreover, the ion angular distribution becomes narrow, with respect to the case without the magnetic field, along the normal to the target direction.

Our investigations demonstrated that if the magnetic field produces electron trapping, its presence may cause a different spatial distribution of charges in front of the irradiated target, with a consequent change of the electric field developed at the frontier of the plasma plume. In addition, axial magnetic field, produced by a permanent magnet, of 0.1 Tesla intensity, has an inversion outside that change significantly the electron path. The electric field generated inside the non-equilibrium plasma can be modified by the external applied magnetic field so that an increment of the ion energy and of the ion current can be obtained, as it will be presented and discussed in this work.

2. INSTRUMENTATION AND METHODS

Nd:Yag laser, 1064 nm wavelength, 9 ns pulse width, 800 mJ maximum pulse energy, and 30 Hz repetition rate was employed to irradiate solid metallic targets at 10^{-7} mbar vacuum pressure. A lens placed in air, outside of the vacuum chamber, focuses the laser light, through a thin glass window, on the target surface with a spot size of 1 mm^2. The incidence angle of the laser beam is 56°, at which the laser spot size is 1.78 mm^2. For this experiment, the laser pulse energy was limited to 300 mJ to which correspond an intensity of 1.7×10^9 W/cm^2.

The irradiated targets were pure Al, Cu, and Ta sheets, 2 cm × 2 cm surface and 3 mm thickness. A scheme of the experimental setup employed in this experiment is reported in Figure 1. An axial permanent magnet with a hallow

cylinder and dimensions 14 cm length, 23.2 cm external diameter, and 15.0 cm internal diameter was placed inside the vacuum chamber. The magnetic axis is placed along the normal to the target surface (z direction) at the laser spot position. This is also the direction of the magnetization vector of the NdFeB permanent magnets enclosed in the cylindrical assembly. Inside to the cylinder, the magnet produces field lines parallel to the cylinder axis with a maximum intensity of 0.1 Tesla, constant over 10 cm length, while externally, along the z axis, the field intensity decreases up to a negative value of −300 Gauss, and than grows again to zero. Along the z axis, the iso-level field lines are closed forming a minimum B module, |B| = 0, at 3.5 cm distance from the cylinder bases. Figure 2a shows a scheme of the magnet setup reporting the geometry of the field with the magnetic iso-level curves (the field lines are orthogonal to the iso-level curves) at different values of B. Figure 2b reports the magnetic field module, |B|, versus the z distance from the target surface up to the detector place (ion collector (IC) position). It is possible to observe two points of |B| = 0 at which the sign of the B field changes. The permanent magnet photo is reported in the inset of Figure 1b. More details on this magnet are given in Ciavola *et al.* (2004). The target surface is placed at 3 cm distance from the first |B| = 0 point, which will have an important role in this investigation, and the IC detector is placed at 63 cm from the target surface, where the magnetic field is negligible (B = −10 Gauss).

A Faraday cup 10 cm long, with a −100 V biased IC and electron suppression grid, is used at different distances from the targets along the magnet axis normal to the target surface. The IC collector was placed at the following target distances: 50, 63, 76, and 89 cm. IC measurements were performed with and without the magnetic field. A fast storage oscilloscope, 1 MHz frequency and 50 Ω input resistor, was employed to record the IC ion spectra and to calculate, from the TOF measurements, the mean velocities and
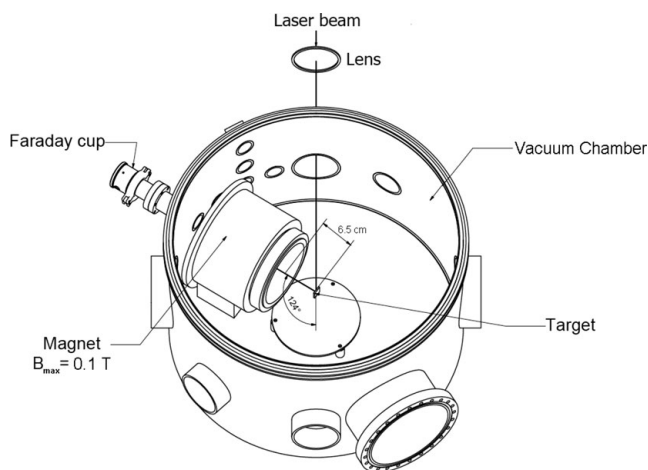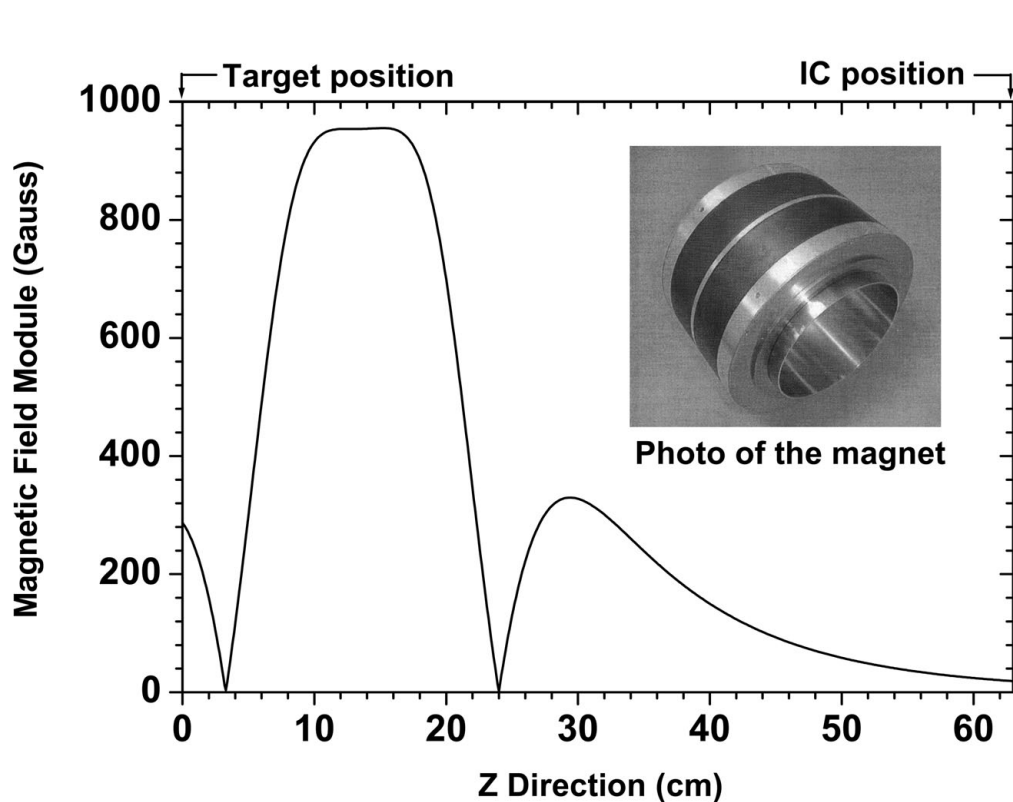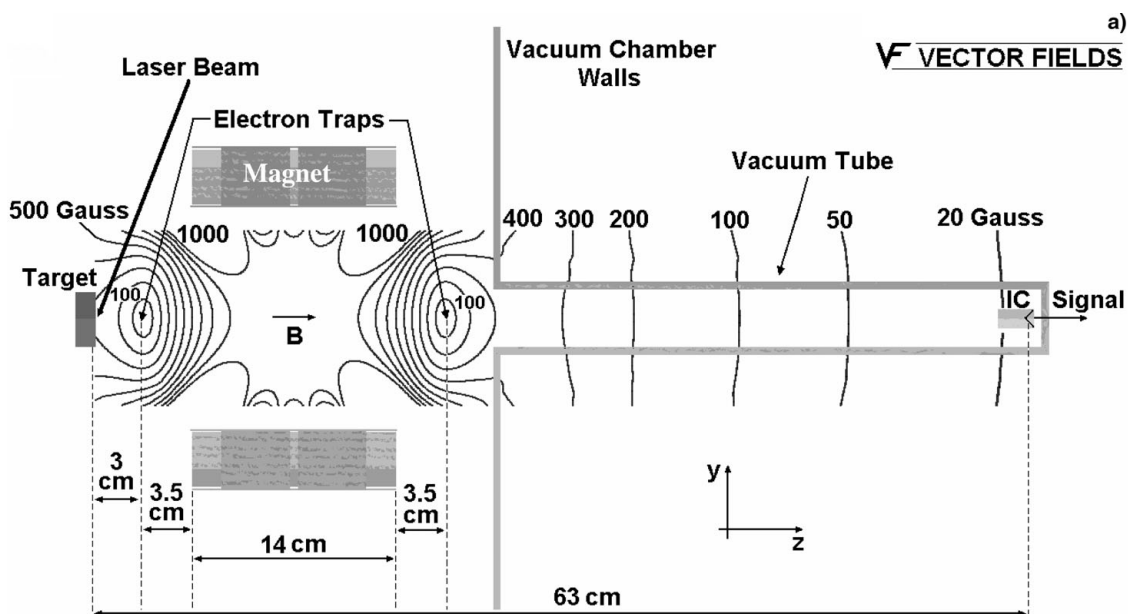

Fig. 1. Scheme of the experimental setup.

Fig. 2. Scheme of the iso-level magnetic field of the experimental set-up (**a**) and axial magnetic field module versus normal distance from the target surface (**b**) (inset: magnet photo).

kinetic energies of detected ions. Ion spectra analysis was performed by using the "Peakfit" code, in order to analyze the IC spectra with Boltzmann functions for the different ion groups ejected from the plasma (http://cranessoftware. com/products/systat/2006). The mathematical deconvolution process permitted to measure the mean ion energy as a function of the ion charge state and laser intensity, in order to calculate the ion yields and the ion energy shifts and, finally, to evaluate the plasma temperature. The "Opera 3D" code (http://www.vectorfields.com/content/ view/26/49) was employed to perform the computer simulation of particles trajectories into electro-magnetic fields.

The ion and electron path simulations were of interest to understand the mechanisms of generation, development and kinetics of laser-generated plasma in vacuum, as it will be discussed in the following. Data analysis were compared to our previous measurements of ion TOF performed with an ion energy analyzer (IEA) giving, from electrostatic deflection, energy and charge state of the ions ejected from Al, Cu, and Ta targets during laser ablation. More details on the TOF-IEA measurements are reported in the reference articles (Torrisi *et al.*, 2002, 2003, 2006*a*).

3. RESULTS

Figure 3 reports a comparison between some typical IC spectra detected along the normal direction to the target surface obtained ablating Al, Cu, and Ta in similar conditions (laser energy between 140 and 300 mJ, 56° incident angle, 63 cm IC-target distance, 1 mm^2 spot size, 10^{-7} mbar pressure), without (a, c, e) and with (b, d, f) the axial magnetic field application. Spectra show the laser photo-peak (start signal at zero TOF) and the large positive IC ion signals (stop signal) permitting thus to measure the
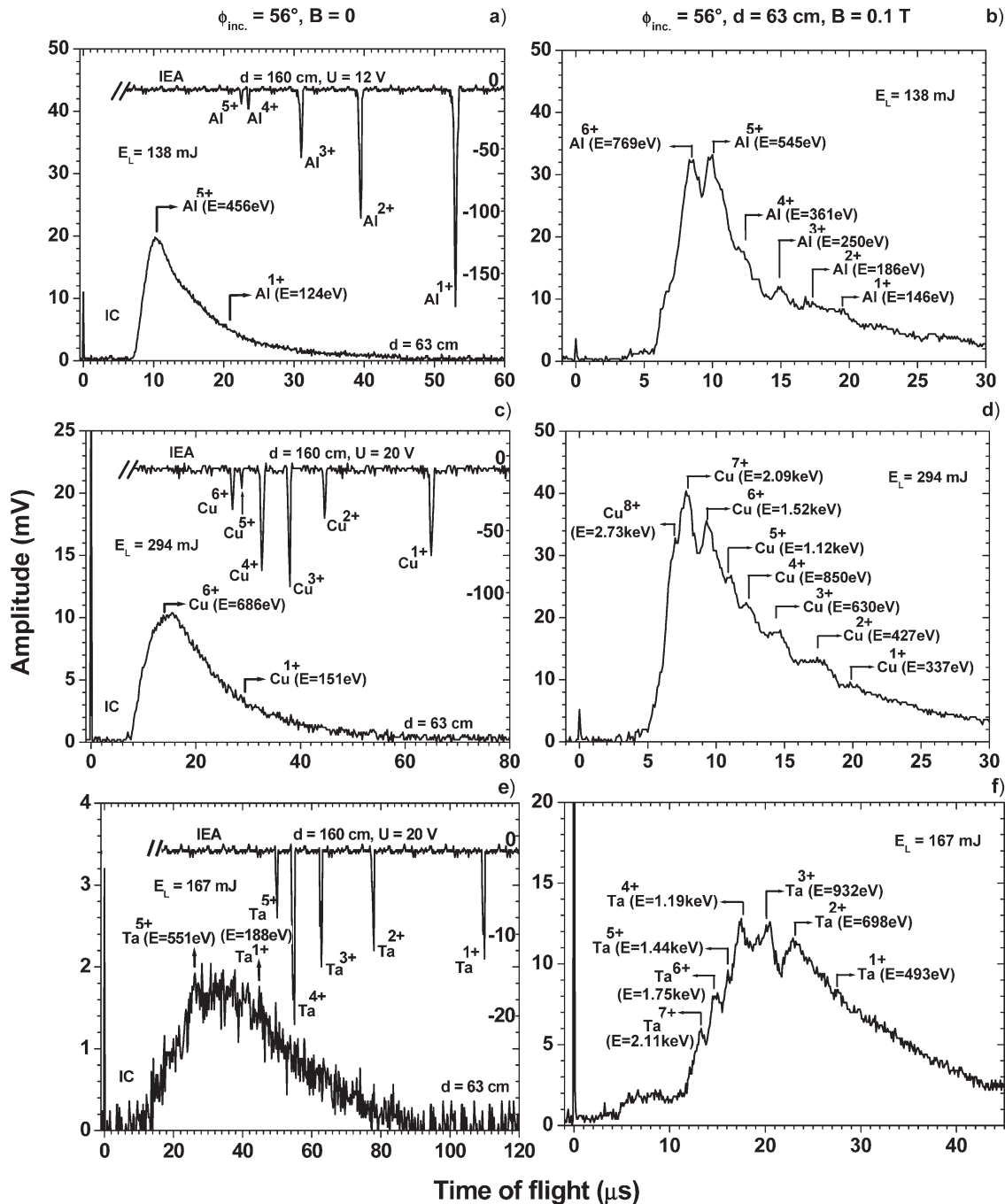

Fig. 3. Comparison of TOF ion spectra from IC and IEA without (**a**, **c**, **e**) and with (**b**, **d**, **f**) magnetic field.

average TOFs, ion velocities and ion energies. Previous IEA measurements demonstrated that, in the same experimental conditions, the detected charge states were 5+ for Al at 138 mJ, 6+ for Cu at 294 mJ, and 5+ for Ta at 167 mJ, as presented in literature (Torrisi *et al.*, 2002, 2003, 2006*a*). The TOF-IEA spectra are reported, as narrow negative peaks, in the top of the Figures 3a, 3c, and 3e for Al, Cu and Ta ablation, respectively. IEA measurements were performed at the same laser intensities used in this experiment; the ions were detected at 160 cm distance from the target and the potential of deflection, U, used to select the ion energy-to-charge ratio, was fixed in the range 12–20 V to selects an energy-to-charge ratio between 90 to 200 eV/charge state. Thus, assuming that such charge states are obtainable without magnetic field and by observing the spectra detected in presence of axial magnetic field application, the IC spectra deconvolution by the Peakfit code permitted to evaluate, with a good approximation, the energy of the different detected ion charge states. Figure 4 shows an example of IC deconvolution process, applied to the Cu ablation at 294 mJ and 0.1 Tesla magnetic fields, reporting eight ion charge states. TOF-IEA spectra obtained without magnetic field show only six charge states for the Cu ions. TOF-IC spectra without magnetic field don't show well-separated ion charge states and the applied deconvolution process indicates an energy of about 151 eV for Cu^{1+}, and an energy of about 686 eV for Cu^{6+}. Thus, the comparisons reported in Figure 3 demonstrate that a significant difference occurs in the TOF spectra acquired without and with the axial magnetic field application. Three main differences concern the following points: (1) the ion distributions become more energetic in presence of the magnetic field; (2) the integral ion yield (ion charge) increases with the magnetic field application; (3) the ion charge states increase with the use of magnetic field; (4) the spectra are better resolved in TOF
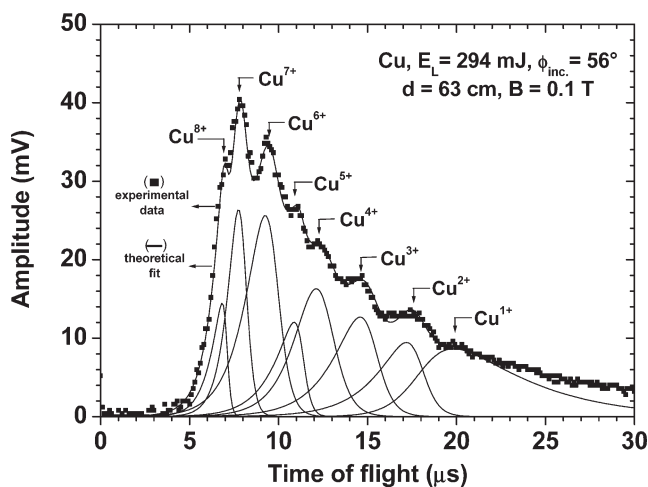
with the use of the magnetic field with respect to the case without the field.

We analyze in detail the above four points. (1) The TOF spectra permit to calculate the ion velocities and energies. The average ion energies for the three ablated elements increase for the ions generated in presence of the magnetic field with respect to the without case. Figure 5a reports the mean ion energies for the ion spectra of Figure 3 versus the charge state. At high laser energy, applying the magnetic field, the charge state 1+ gets an average energy increment of the order of 18%, 122%, and 161% for the Al, Cu, and Ta ions, respectively, while the charge state 5+ endures an increment of about 19%, 123%, and 162% for Al, Cu, and Ta ions, respectively. This result demonstrates that the ion energy increment due to the application of the magnetic field is not dependent on the ion charge state. This effect is due to the increment of the equivalent voltage, V_0, producing ion acceleration inside the non-equilibrium laser-generated plasma (Torrisi & Gammino, 2006; Davis *et al.*, 1999). Due to the electron trapping at 3 cm distance from
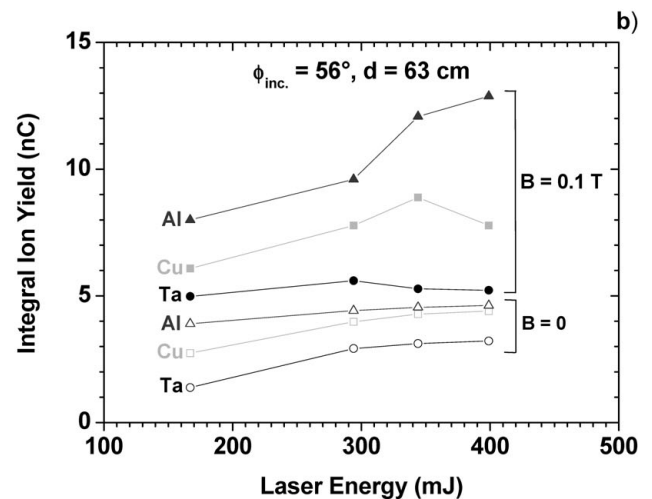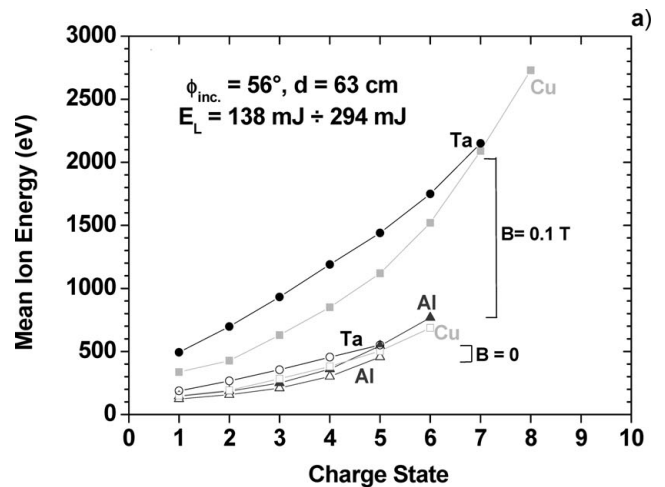
Fig. 4. Typical Peakfit deconvolution process of TOF spectrum for Cu ion detection.

Fig. 5. Mean ion energy versus ion charge state (**a**) and integral ion yield versus laser energy (**b**) for conditions without and with magnetic field.

the target surface, in fact, a further electrostatic potential, V_0', is responsible of further ion acceleration along the z direction. Probably the low increment of the Al ion energy with respect to the copper and Ta is due to the lower electron density of this element, in agreement with ion energy dependences reported in previous investigations.

(2) The integral ion yield, proportional to the area of the TOF signal, represents an indication of the ion current directed toward the IC detector. It decreases from Al to Cu and to Ta for both cases, with and without magnetic field,

due to the different melting point of the three elements, lower for Al (660°C) and Cu (1083°C) and higher for Ta (2996°C). The integral ion yield increases in presence of the magnetic field with respect to the case without the field, as described in Figure 5b. It is for higher maximum for laser energy; 400 mJ, the increment is higher than 100% for Al, Cu, and Ta with respect to the case without magnetic field. A detailed comparison of TOF spectra relative to Ta ablation, with and without the magnetic field at different laser energies, is reported in Figure 6. This figure
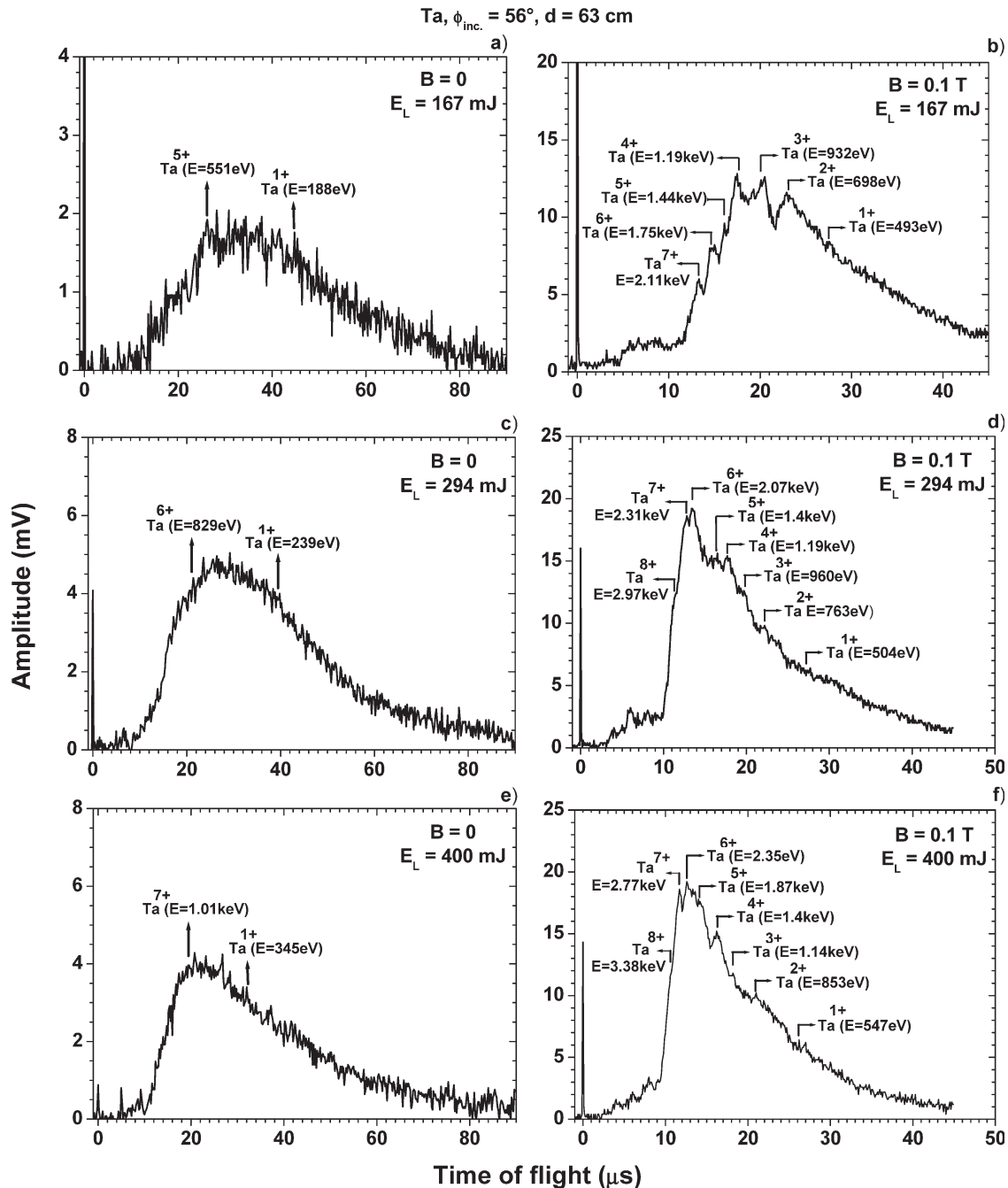

Fig. 6. TOF spectra comparison for Ta detection without (**a**, **c**, **e**) and with (**b**, **d**, **f**) magnetic field as a function of the laser energy.

shows that the magnetic field produces a significant ion focalization observable as a maximum integral ion yield of Ta ions, at 63 cm target-IC distance, and 294 mJ laser energy. At other energies the yield decreases. This phenomenon is present for the three investigated materials but, at 63 cm distance, it occurs at different values of the laser energy: 344 mJ for Cu and 400 mJ for Al, as reported in Figure 5b. This result is due to the magnetic and electric focalization of the ions towards the IC position. The ion deflection is caused by the high density of the electron cloud localized in the magnetic electron trap ($|B| = 0$) at 3 cm distance from the target. This negative cloud acts such as a negative biased deflector for the tangential ion trajectories which are deflected toward the IC position increasing the ion current. Of course, by increasing the IC-target distance, the integral ion yield decreases, due to the decrement of the solid detection angle, as reported in the data of Figure 7, showing that the best focalization occurs at 63 cm distance from the target.

(3) A clear increment of the charge state is obtained by generating the laser plasma in the axial magnetic field. In fact, by comparing experimental data with previous IEA measurements, results demonstrated that the ion charge states increase from 5+ up to 6+ for Al, from 6+ to 8+ for Cu, and from 5+ to 7+ for Ta. This result is due to the increment of the electron-ion interactions when the magnetic field generates the electron trap in front of the target surface. Not only ions cross and collide with more electrons along their path, especially at the electron trap place, but also during their target-trap flight, due to a large number of back-scattered electrons from the trap, as demonstrated by the computer simulation code. The increment of the electron-ion collisions increases the ionization processes producing higher ion yields and ion charge states. Shortly, we can assume that the electrons in the trap act as a stripper for the out coming ions.

(4) Figure 8a reports the TOF spectra resolving power, calculated as TOF/ΔTOF ratio, versus laser energy for the three ablated targets. It shows a resolution decrement with the laser energy for the three elements and a better resolution obtainable for ions with low energy. Moreover, the figure indicates that heavy elements are better resolved in TOF with respect to light elements, demonstrating that the resolution depends significantly on the charge-to-mass ratio of ejected ions, according to the general Lorentz law. The resolving power depends also on the IC-target distance because the TOF ion detection separates the ion charge states differently at different distances. An optimum resolution distance
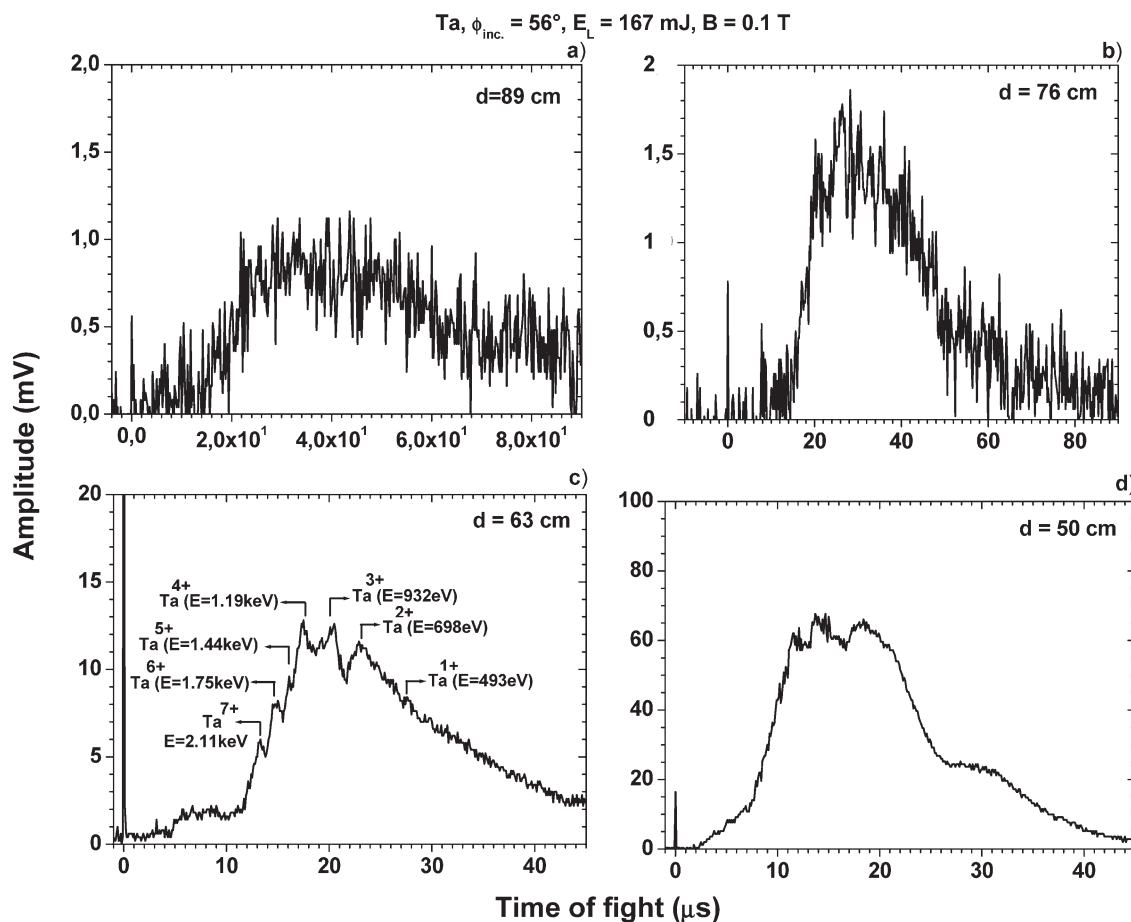

Fig. 7. TOF spectra comparison for Ta detection under magnetic field as a function of the target-IC distance.

of 63 cm was found for the three elements irradiated at 138 mJ (Al), 294 mJ (Cu), and 167 mJ (Ta), while at other distances the peak separation decreases, as reported in Figure 8b.

In order to explain the obtained results and to better understand some mechanisms of ion acceleration occurring inside the laser-generated plasma, useful simulations of ion and electron trajectories were investigated by using the Opera 3D simulation code. Without the magnetic field, the electron and ion streams are ejected from the plasma with linear trajectories starting from the laser spot size with maximum divergence angle of about $\pm 45°$ for Al, $\pm 40°$ for Cu, and $\pm 30°$ for Ta, centered with the normal to the target surface, according to previous measurements of angular distribution (Torrisi *et al.*, 2001). The simulations use a Monte Carlo method with ions and electrons having Boltzmann distributions with mean energies of the order of 1 keV and 100 eV, respectively. The magnetic field has a strong influence on the electron trajectories which show helicoidal shape geometry and trapping at the $|B| = 0$ positions,

while its influence is negligible on the ion trajectories, as reported in Figures 9a and 9b, respectively.

The simulations, performed with 600 electrons and ions, show that the electron trapping produces an increase of the electron density at 3 cm distance from the target surface, along the z direction, as reported in Figure 10a. The density depends strongly on the space and on the time. Its maximum value in the space is at about 3 cm from the target surface and its thickness is about 1 cm. The computer simulation indicates that the electron cloud is approximately 2.5 cm far from the target surface, it has a thickness of about 1 cm, and a circular shape (about 3 cm radius, see inset of Fig. 9a). This negative cloud generates a strong electric field in front of the target that accelerates the ions along the z direction. Moreover, the electron cloud produces electron backscattering toward the target, which increases further the number of ionization processes, and also the average charge state through a step-by-step process. The electron density of the cloud attains the maximum value about 10 ns after the laser shot, and it maintains high values for about 150 ns, then decreasing down to 10% of the maximum at a time on the order of 300 ns, when the effect of the ion acceleration becomes negligible, as shown in the simulation plot of density versus time reported in Figure 10b. Thus the ion acceleration due to the presence of the magnetic field has duration of the order of 300 ns.

TOF-IC measurements give information about the electron plasma temperature and the Coulomb ion acceleration produced by the plasma pulse. In the following, the two contributions, thermal and Coulombian, are evaluated at a first approximation, for the spectra reported in Figure 3. Assuming that the ions with the higher charge have a kinetic energy due mainly to Coulomb interactions rather than thermal one, it is possible to imagine the following scenario for the measurements taken without magnetic field application: By subtracting from the Al^{5+} ion energy of 456 eV the Al^{1+} ion energy of 124 eV, and by dividing the resulting 332 eV energy by the corresponding $4+$ charge state difference, an equivalent accelerating voltage of 83 V is found, indicating that the thermal contribution energy for this plasma is 41 eV, obtainable so as a difference between the first ionized specie energy (124 eV), and the Coulomb energy of this specie (83 eV). By subtracting from the Cu^{6+} ion energy of 686 eV the Cu^{1+} ion energy of 151 eV, and by dividing the resulting 535 eV energy by the corresponding $5+$ charge state difference, an equivalent accelerating voltage of 107 V is found, indicating that the thermal contribution energy for this plasma is 44 eV, obtainable so as a difference between the first ionized specie energy (151 eV) and the Coulomb energy of this specie (107 eV). By subtracting from the Ta^{5+} ion energy of 551 eV the Ta^{1+} ion energy of 188 eV, and by dividing the resulting 363 eV energy by the corresponding $4+$ charge state difference, an equivalent accelerating voltage of 90.8 V is found, indicating that the thermal contribution energy for this plasma is 97.2 eV, obtainable so as a difference
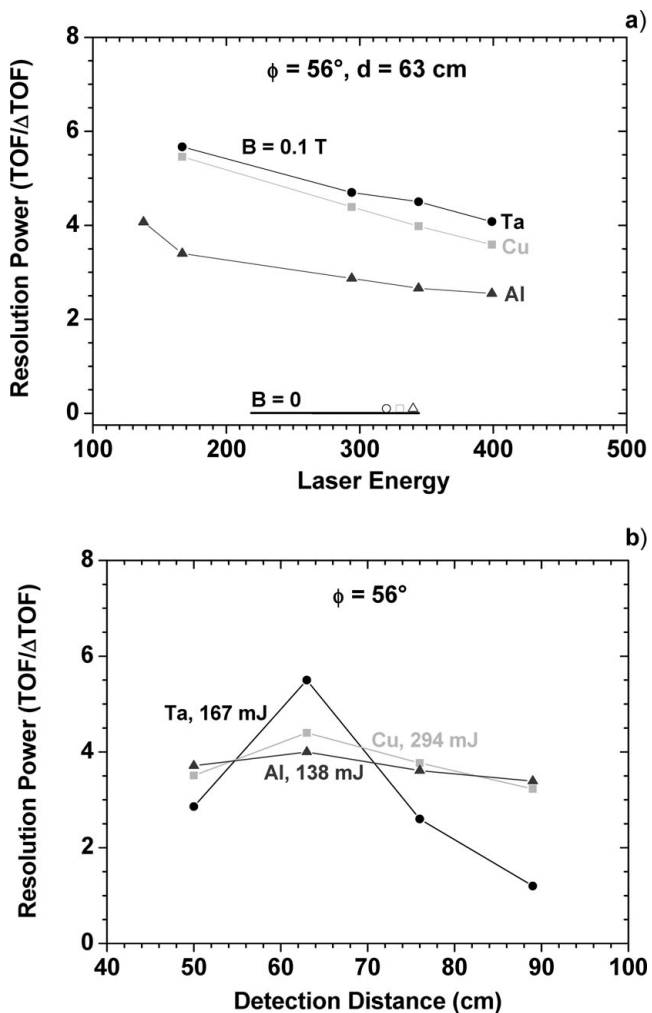
Fig. 8. Resolution power as a function of the laser energy (**a**) and as a function of the target-IC distance (**b**) for the different metals ablation with and without magnetic field.
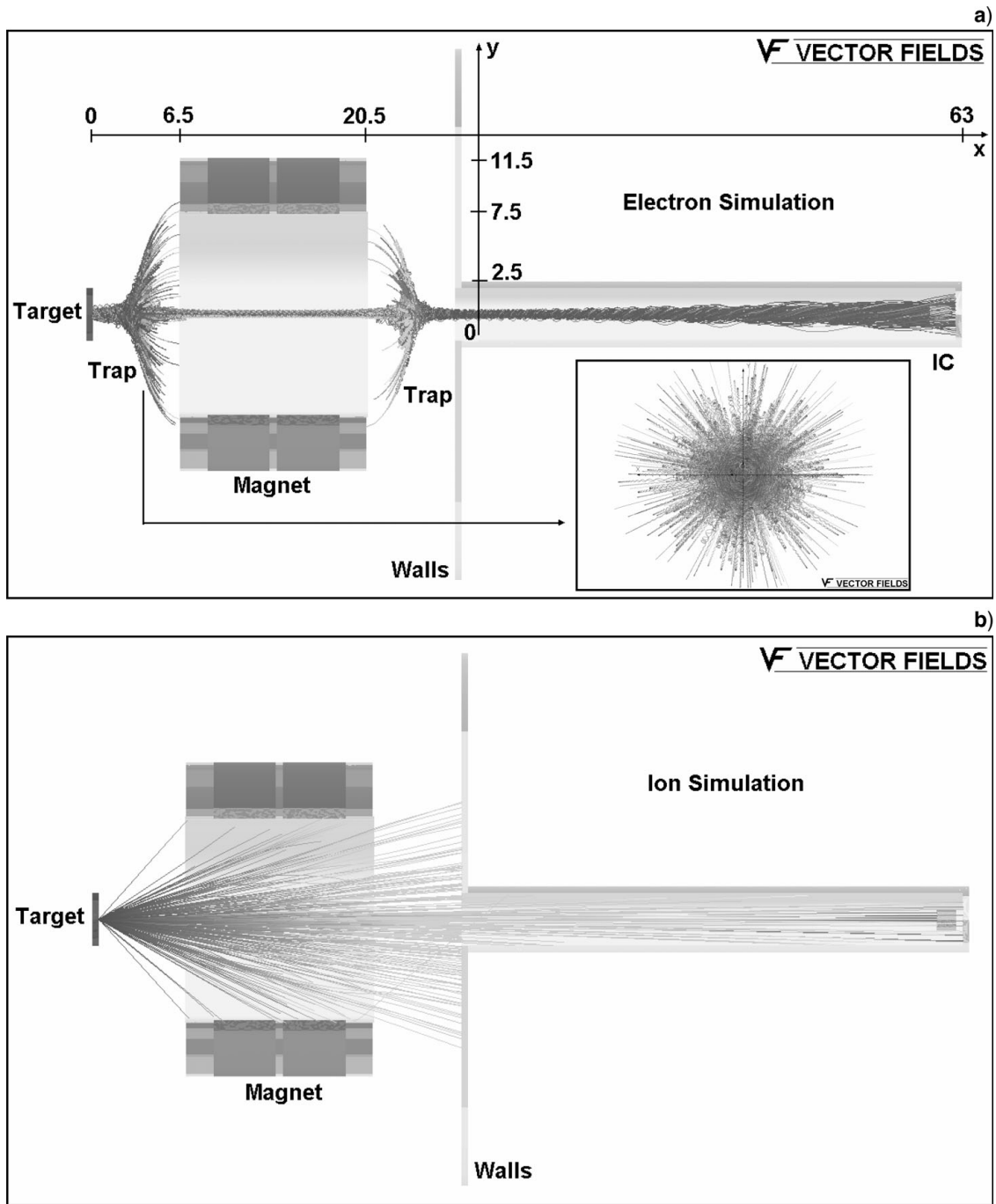
Fig. 9. Opera 3D simulation of electron trajectories (**a**) and ion trajectories (**b**) for particles produced by the laser-generated plasma in presence of magnetic field.

between the first ionized specie energy (188 eV) and the Coulomb energy of this specie (90.8 eV). Thus, in absence of magnetic field, the electron plasma temperature of 41 eV, 44 eV, and 97 eV is evaluated for Al, Cu, and Ta plasma, respectively and an equivalent acceleration voltage, V_0, of 83 V, 107 V, and 91 V can be associated to the Al, Cu, and Ta plasma, respectively. Such results indicate that the plasma temperature increases from Al to Cu and to Ta, in agreement with the electron density of the plasma which increases with the atomic number of the ablated metallic specie. These temperatures are in reasonable agreement with the theoretical previsions obtainable using the following empirical relationship (Torrisi *et al.*, 2006*b*):

$$kT_e(keV) = 6 \times 10^{-5}[I(W/cm^2)\lambda(\mu m)^2]^{1/3} \qquad (1)$$

where k is the Boltzmann constant, T_e is the electron temperature, I is the laser pulse intensity, and λ is the laser wavelength.
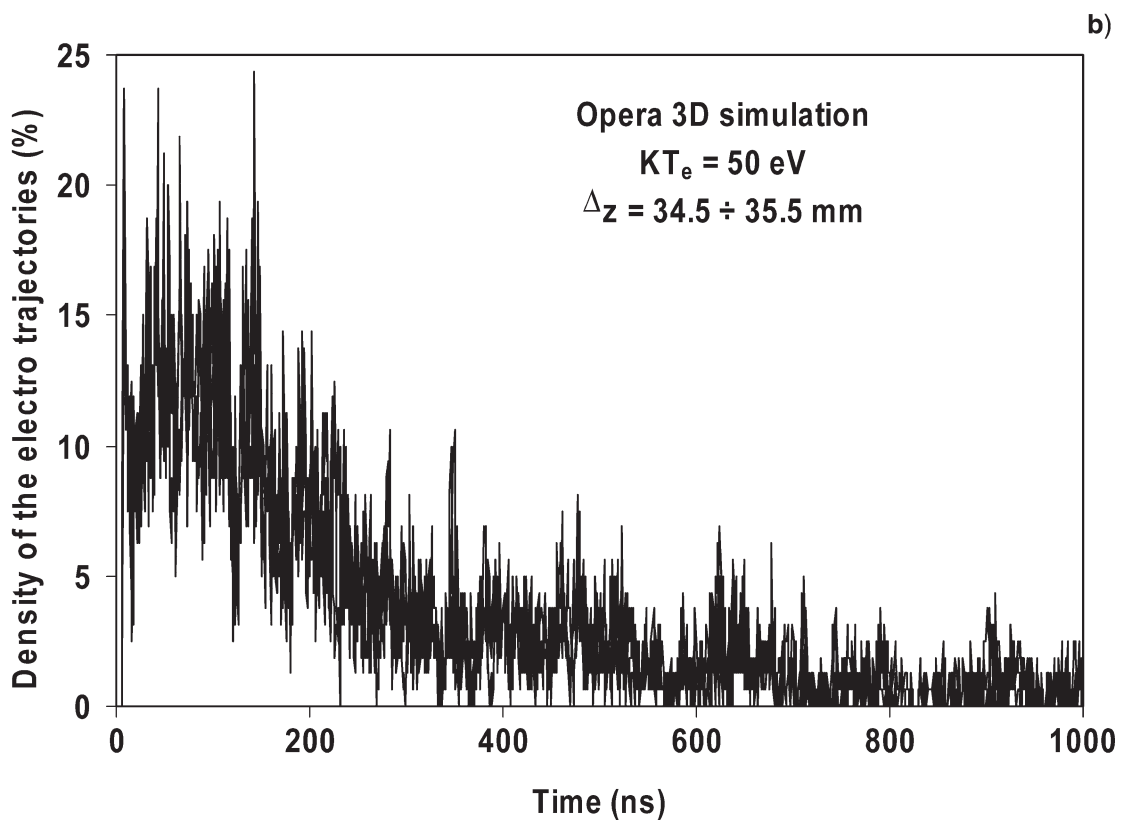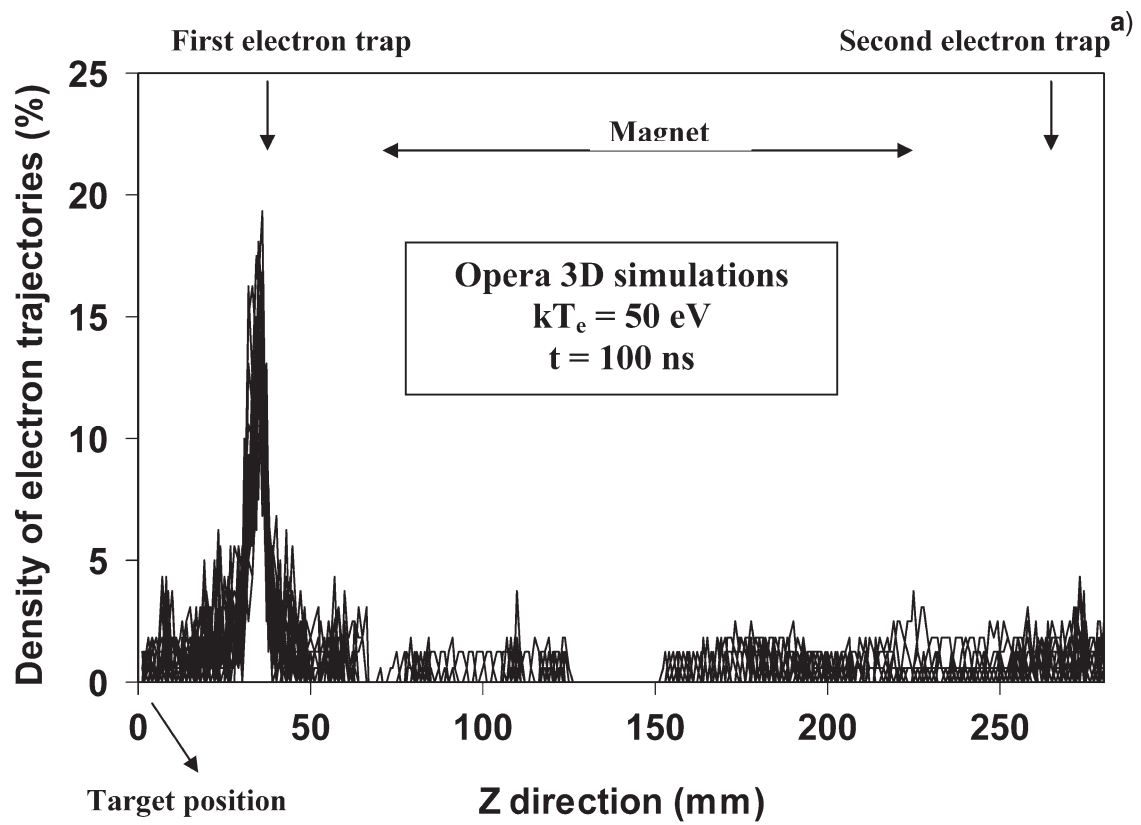
Fig. 10. Opera 3D simulation of the electron density versus z direction (**a**) and TOF time (**b**).

Eq. (1) gives a temperature of 59 eV, 77 eV, and 63 eV for Al (at 138 mJ), Cu (at 294 mJ), and Ta (at 167 mJ), respectively.

Assuming the average plasma electron temperature to be on the order of 50 eV and the plasma electron density to be on the order of $10^{16}/cm^3$, according to literature (Torrisi *et al.*, 2006*c*), the consequent Debye length, obtainable in condition of a local thermal equilibrium (LTE) (Chen, 1994), is about 0.5 μm. Thus, in absence of external magnetic field, assuming the equivalent acceleration voltage V_0, on the order of 100 V, to be applied to the Debye distance, the corresponding electric field due to the laser shot producing plasma is of the order of 2 MV/cm, in good agreement with literature (Torrisi & Gammino, 2006). This electric field acts during a time comparable with the laser pulse duration, i.e., about 10 ns.

By assuming that the above plasma temperatures for the plasma are maintained with the application of the magnetic field, the application of the axial magnetic field increases significantly the Coulomb ion acceleration effect. In facts, the equivalent acceleration voltage, V_0', calculable is 105 V, 293 V, and 396 V for Al, Cu, and Ta, respectively, as obtainable by the differences between the first ionized ion energy and the plasma temperature.

By excluding the thermal energy contribution, the increment of the ion acceleration voltage along the z direction is thus:

$$\Delta V_0 = V_0' - V_0 \qquad (2)$$

where ΔV_0 represents the increment of the equivalent voltage acceleration in presence of the magnetic field, V_0' represents the total equivalent voltage acceleration in presence of magnetic field and V_0 represents the equivalent voltage in absence of the magnetic field. ΔV_0 assumes the value of 22 V, 186 V, and 305 V for Al Cu, and Ta plasma, respectively. Assuming this potential to be applied to the target-electron trap (electron cloud) distance of about 2.5 cm, the accelerating electric field due to the electron trap assumes the value of 8.8 V/cm, 74.4 V/cm, and 122 V/cm in the three cases, respectively.

Although the electric field due to the presence of the electron cloud in the trap in front of the target is five or six order of magnitude lower with respect to the electric field generated by the laser shot, its influence on the ions is very important because it acts over a larger time during the expansion of the plume. In fact this electric field due to the electron trapping effect accelerates ions over 2.5 cm and for flight travel times of the order of 300 ns.

4. DISCUSSION

The results reported in this article have shown the increment of the plasma ion energy due to the presence of the axial magnetic field. Although a magnetic field cannot accelerate ions, it can perturb the electrical field developed inside the plasma that produces the acceleration of the ions ejected from the non-equilibrium plasma.

The magnetic field value is −300 Gauss at the target surface and increases to zero at 3 cm distance from the target surface. At about 10 cm from the target surface, the magnetic field increases up to 0.1 Tesla. This configuration produces a magnetic trap in front of the target surface, due to the magnetic |B| valley located at 3 cm distance, where the conservation of particle energy and momentum produces a mirror effect for the electrons generating, for times on the order of hundredth nanoseconds, a negative electron cloud. This phenomenon is responsible of the increment of the electric field accelerating the ions, of the increment of the electron-ion interactions, and of the ion deflection towards the IC detector. The electron trapping effect, due to the presence of the magnetic module valley, is observable by the Monte Carlo simulation of the electron trajectories in static electro-magnetic field performed by using the Opera 3D code. Figure 9a shows a simulation of electron trajectories in the used experimental set-up reporting their path in the X-Z plane versus z distance. Such electrons have a Boltzmann distribution with a temperature of the order of 50 eV. The trapping effect occurs also at lower and higher electron energies and it is particularly evident for electrons having velocity component orthogonal to the z direction. The simulation uses an anisotropy electron emission with an angular distribution with an aperture of $\pm 30°$, similarly to that of ions emitted in the same experimental conditions. Of course, electrons with velocity component directs along the axial direction are not trapped.

The charge gradient, between the electron cloud trapped in the magnetic mirror and to the ion cloud, due to the slower emission of ions from the target surface, generates an electric potential inside the non-equilibrium plasma increasing the existent electric field responsible of the ion acceleration along the target normal direction.

Moreover, the computer simulation demonstrated that a large number of electrons are backscattered from the trap, an effect that can be responsible of a further increment of the electron-ion collisions. Thus, further ionization processes increase the ion charge states.

Similarly, Figure 9b shows the simulation trajectories due to Ta ions, with a charge state from 1+ to 7+, and an energy distribution following the "Coulomb-Boltzmann shifted" distribution given in previous articles (Torrisi *et al.*, 2002). IC measurements for Ta, in agreement with the theory reported in this reference, give ion energies ranging between 500 eV, and 2 keV for the charge states going from 1+ to 7+, respectively. The simulation uses an anisotropy ion emission with an angular distribution with an aperture of $\pm 30°$, according to literature (Torrisi *et al.*, 2001). The simulation shows that the electrons trajectories are strongly modified by the magnetic field while the ions trajectories modifications are negligible.

The Monte Carlo simulation permitted to put in evidence the electron density versus the distance from the target

surface (Fig. 10a) and versus the TOF time (Fig. 10b). This latter study, obtained simulating the ion trajectories emitted by 600 electrons at 50 eV electron temperature, demonstrates that the intense electron trap at 3 cm distance from the target surface has an extension of about 10 mm in z direction, as reported in Figure 10a by fixing the time at 100 ns from the laser shot and reporting the electron density for 1 ns time duration. This large cloud extension increases the electric field because the ion acceleration potential results applied to a lower target-electron cloud distance. Moreover, the higher electron density generated by the magnetic trap occurs at about 10 ns TOF time from the laser shot, in agreement with expected times and has a duration of about 300 ns or more. The simulations of Figure 10b demonstrates, in fact, that, by fixing the attention on the electron density in 1 mm Δz width, from 34.5 to 35.5 mm at the mirror place, the density remains high for long times of the order of hundreds ns, i.e. sufficiently to increase significantly the ion velocity and the mean ion charge state.

ACKNOWLEDGEMENT

REFERENCES

ALTI, K. & KHARE, A. (2006). Low-energy low-divergence pulsed indium atomic beam by laser ablation. *Laser Part. Beams* **24**, 47–53.

ANDERSON, M., GARATE, E., ROSTOKER, N., SONG, Y., VAN DRIE, A. & BYSTRITSKII, V. (2005). Propagation of intense plasma and ion beams across B-field in vacuum and magnetized plasma. *Laser Part. Beams* **23**, 117–129.

BEILIS, II. (2007). Laser plasma generation and plasma interaction with ablative target. *Laser Part. Beams* **25**, 53–63.

CHEN, L.C. (1994). Particulates generated by pulsed laser ablation. In *Pulsed Laser Deposition of Thin Films* (Chrisey D.B. and Hubler G.K., Eds.), Chap. 6, pp. 167–198. New York: J. Wiley & Sons.

CIAVOLA, G., CELONA, L., GAMMINO, S., PRESTI, M., ANDÒ, L., PASSARELLO, S., ZHANG, X.Zh., CONSOLI, F., CHINES, F., PERCOLLA, C., CALZONA, V. & WINKLER, M. (2004). A version of the trasco intense proton source optimized for accelerator driven system purposes. *Rev. Sci. Instr.* **75**, 1453–1456.

DAVIS, J.R., BELL, A.R. & TATARAKIS, M. (1999). Magnetic focusing and trapping of high-intensity laser-generated fast electrons at the rear of solid targets. *Phys. Rev. E* **59**, 6032–6036.

DUCRUET, C., KORNILOV, N., DE JULIAN FERNANDEZ, C. & GIVORD, D. (2006). Laser generated plasmas characterized under magnetic field. *Appl. Phys. Lett.* **88**, 044102–044104.

GIULIETTI, D. & GIZZI, L.A. (1998). X-ray emission from laser-produced plasmas. *Riv. Nuovo Cimento* **21**, 1–92.

JUNGWIRTH, K. (2005). Recent highlights of the PALS research program. *Laser Part. Beams* **23**, 177–182.

LASKA, L., JUNGWIRTH, K., KRASA, J., KROUSKY, E., PFEIFER, M., ROHLENA, ULLSCHMIED, J., BADZIAK, J., PARYS, P., WOLOWSKI, J., GAMMINO, S., TORRISI, L. & BOODY, F.P. (2006). Self-focusing in processes of laser generation of highly-charged and high-energy heavy ions. *Laser Part. Beams* **24**, 175–179.

SCHAUMANN, G., SCHOLLMEIER, M.S., RODRIGUEZ-PRIETO, G., BLAZEVIC, A., BRAMBRINK, E., GEISSEL, M., KOROSTIY, S., PIRZADEH, P., ROTH, M., ROSMEJ, F.B., FAENOV, A.Y., PIKUZ, T.A., TSIGUTKIN, K., MARON, Y., TAHIR, N.A. & HOFFMANN, D.H.H. (2005). High energy heavy ion jets emerging from laser plasma generated by long pulse laser beams from the NHELIX laser system at GSI. *Laser Part. Beams* **23**, 503–512.

TORRISI, L. & GAMMINO, S. (2006). Method for the calculation of electrical field in laser-generated plasma for ion stream production. *Rev. of Sci. Instr.* **77**, 03B707–03B710.

TORRISI, L., ANDÒ, L., CIAVOLA, G. & BARNÀ, A. (2001). Angular distribution of ejected atoms from Nd:YAG laser irradiating metals. *Rev. Sci. Instr.* **72**, 68–72.

TORRISI, L., CARIDI, F., MARGARONE, D., PICCIOTTO, A., MANGIONE, A & BELTRANO, J.J. (2006a). Carbon plasma produced in vacuum by 532 nm-3 ns laser pulses ablation. *Appl. Surf. Sci.* **252**, 6383–6389.

TORRISI, L., CARIDI, F., PICCIOTTO, A. & BORRIELLI, A. (2006b). Energy distribution of particles ejected by laser-generated aluminium plasma. *Nucl. Instr. Meth. Physics Res. B* **252**, 183.

TORRISI, L., GAMMINO, S., ANDÒ, L. & LASKA, L. (2002). Tantalum ions produced by 1064 nm pulsed laser irradiation. *J. Appl. Physics* **91**, 4685–4692.

TORRISI, L., GAMMINO, S., ANDÒ, L., NASSISI, V., DORIA, D. & PEDONE, A. (2003). Comparison of nanosecond laser ablation at 1064 and 308 nm wavelength. *Appl. Surf. Sci.* **210**, 262–273.

TORRISI, L., RYC, L., MARGARONE, D. & BORRIELLI, A. (2006c). Soft X-ray radiation from metal targets at interaction of 9-ns laser pulses. *Czech J. Phys.* **56**, B571–B579.

WOLOWSKI, J., BADZIAK, J., IVANOVA-STANIK, I., PARYS, P., STEPNIEWSKI, W. & WORYNA, E. (2004). Magnetic field influence on laser-produced ion stream. *Rev. Sci. Instr.* **75**, 1353–1356.

WOLOWSKI, J., CELONA, L; CIAVOLA, G; GAMMINO, S., KRASA, J., LASKA, L., PARYS, P., ROHLENA, K., TORRISI, L. & WORYNA, E. (2002). Expansion of tungsten ions emitted from laser-produced plasma in axial magnetic and electric fields. *Laser Part. Beams* **20**, 113–118.